International Journal of Pharmaceutics: X 11 (2026) 100563

Contents lists available at ScienceDirect

International Journal of Pharmaceutics: X

journal homepage: www.sciencedirect.com/journal/international-journal-of-pharmaceutics-x

Scalable microfluidic fabrication of optimized phospholipid nanocarriers for enhanced topical bioavailability: Analytical QbD integration and *ex vivo* skin permeation assessment

Giulia Bucciarelli [a,b], Giulia Curzi [b], Mattia Tiboni [a], Annalisa Aluigi [a], Andrea Heinz [c], Luca Casettari [a,*]

[a] Department of Biomolecular Sciences, University of Urbino Carlo Bo, Via Ca le Suore 2, 61029 Urbino, PU, Italy
[b] Prosopika srl, Via del Trabocchetto, 1, 61034 Fossombrone, PU, Italy
[c] LEO Foundation Center for Cutaneous Drug Delivery, Department of Pharmacy, University of Copenhagen, 2100 Copenhagen, Denmark

ARTICLE INFO

Keywords:
3D printing
Fused deposition modeling (FDM)
Topical drug delivery systems
IVRT
Vertical diffusion cell
Design of Experiment (DoE)

ABSTRACT

18β-Glycyrrhetinic acid (18β-GA), the primary bioactive metabolite of glycyrrhizin (GL) derived from licorice root, exhibits anti-inflammatory, antioxidant, and antimicrobial activities, as well as excellent biocompatibility, making it a promising candidate for the treatment of dermatological disorders. However, its poor water solubility limits topical bioavailability. In this study, an Analytical Quality by Design (QbD) approach was established to develop and optimize nanocarriers loaded with 18β-GA, to improve skin penetration while providing sustained and controlled release. Ethosomes, glycerosomes, and glycethosomes were produced using an innovative and customized 3D-printed microfluidic chip, resulting in vesicles with controlled size, narrow polydispersity, high encapsulation efficiency, and high physicochemical stability through a reproducible and cost-effective process. A Design of Experiments (DoE) strategy was used to identify critical formulation parameters and develop a predictive mathematical model. The three optimized formulations were incorporated into an alginate hydrogel, exhibiting shear-thinning behavior, ideal for topical application. *Ex vivo* permeation studies revealed that the optimized nanocarriers modulate the skin delivery of 18β-GA, with formulation composition significantly influencing drug distribution profiles. The systems reduced rapid diffusion into the receptor phase and promoted controlled drug release, supporting localized delivery. Drug accumulation within the skin layers indicated that release from the formulation represents the rate-limiting step. The hydrogels exhibited prolonged drug release and improved skin contact, enabling sustained and uniform topical application. Process scalability was successfully achieved using a peristaltic pump, highlighting the robustness, low-cost nature, and industrial feasibility of the proposed microfluidic approach for controlled topical drug delivery.

1. Introduction

Plant-derived bioactive ingredients are increasingly recognized for their therapeutic potential in dermatology and cosmetology. Among them, glycyrrhetinic acid (GA), a triterpenoid aglycone derived from glycyrrhizin (GL) in licorice root (*Glycyrrhiza glabra*), has drawn attention for its well-documented anti-inflammatory, antioxidant, and antimicrobial properties (Kowalska and Kalinowska-Lis, 2019; Pastorino et al., 2018; Shinu et al., 2023; Yamaguchi et al., 2010). 18β-glycyrrhetinic acid (18β-GA) is the principal active stereoisomer of GA and represents the main contributor to biological and pharmacological effects of licorice extracts (Lin et al., 2024; Bag and Majumdar, 2012; Sun et al., 2018; Cai et al., 2022). Structurally related to corticosteroids, 18β-GA can modulate inflammatory pathways, suppress cytokine production, inhibit tyrosinase activity, reducing UVB-induced erythema and hyperpigmentation, and regulate the abnormal expression of metalloproteinases (Li et al., 2019; Saha et al., 2015; Wang et al., 2013; Quan et al., 2021). Moreover, 18β-GA exhibits excellent skin tolerability and a favorable safety profile, with allergic contact dermatitis being extremely rare (Kowalska and Kalinowska-Lis, 2019; Verratti et al., 2011; Wang et al., 2024; Kong et al., 2015; Andersen, 2007). The lipophilic nature and low water solubility of 18β-GA markedly reduce its

* Corresponding author.
E-mail address: luca.casettari@uniurb.it (L. Casettari).

https://doi.org/10.1016/j.ijpx.2026.100563
Received 31 March 2026; Received in revised form 4 May 2026; Accepted 5 May 2026
Available online 6 May 2026

skin bioavailability, thereby restricting its therapeutic potential in dermatological applications. Skin penetration primarily depends on a compound's molecular weight and partition coefficient (log P), which reflects its lipophilicity. The outermost skin layer, the *stratum corneum* (SC), is highly lipophilic and represents the main barrier to penetration. Generally, compounds with log *P* values between 1 and 4 and molecular weights below 500 Da are suitable for transdermal delivery, as defined by *Bos and* Meinardi (Bos and Meinardi, 2000). Although 18*β*-GA has a molecular weight of 470.7 Da, its high log *P* value (6.6) severely limits skin diffusion, highlighting the need for strategies to enhance its permeability (Kowalska and Kalinowska-Lis, 2019; Quan et al., 2021; Tiboni et al., 2020; Raina et al., 2023). Conventional liposomes are often unsuitable for transdermal delivery, as their rigid structure limits penetration into the SC (Albakr et al., 2024; Prow et al., 2011). Ethosomes, composed of phospholipids, water, and high ethanol content (20–45% *v*/v), form soft, flexible vesicles that enhance skin permeation. Ethanol acts as an efficient permeation enhancer by fluidizing the SC lipids and increasing both intercellular and intracellular permeability. These flexible vesicles can traverse narrow skin pores and release the encapsulated drug into deeper skin layers, even though the high ethanol content may cause dehydration, discomfort, and compromise the integrity of the skin lipid barrier (Abdallah et al., 2025; Zahid et al., 2018; Verma and Pathak, 2010). Glycerosomes, composed of phospholipids, water, and 10–50% *v*/v glycerol, were first introduced by *Manca* et al. for diclofenac delivery (Manca et al., 2013). They offer higher encapsulation efficiency, improved SC penetration, and enhanced fluidity and stability. Glycerol, a safe and widely used excipient, acts as an edge activator, increasing bilayer flexibility (Gupta et al., 2020a; Sharma et al., 2023). Glycethosomes, combining ethanol and glycerol, merge the advantages of ethosomes and glycerosomes, improving drug permeation while reducing skin irritation. *Manca* et al. first developed these vesicular systems for clotrimazole delivery (Abdallah et al., 2025; Zhang et al., 2022; Pleguezuelos-Villa et al., 2020; Manca et al., 2019).

In this study, a novel Analytical Quality by Design (QbD) approach was established to develop and optimize nanocarriers loaded with 18*β*-GA. Ethosomes, glycerosomes, and glycethosomes were produced using an innovative 3D-printed microfluidic chip manufactured via fused deposition modeling (FDM), that enable precise control over nanoparticle properties (Rahali et al., 2024; Su et al., 2023). Recent advances in microfluidic technologies and nanoparticle manufacturing have underscored the critical role of controlled production strategies in overcoming the limitations of conventional vesicle preparation methods, particularly in terms of reproducibility and batch-to-batch variability. In this context, microfluidic-assisted fabrication has demonstrated superior control over vesicle size distribution and polydispersity compared to bulk techniques (Duarte et al., 2024; Xu et al., 2025). The customized design allowed the production of vesicles with a spherical morphology and controlled size, narrow polydispersity, and excellent stability, while ensuring cost-effective and reproducible manufacturing (Agha et al., 2023). We systematically applied a Design of Experiments (DoE) strategy to establish predictive mathematical models assessing the influence of formulation variables on particle size and polydispersity index (PDI). The optimized formulations were further evaluated for encapsulation efficiency, long-term stability, and their ability to enhance 18*β*-GA accumulation in the skin via *ex vivo* permeation and retention studies. Finally, we demonstrated the scalable production using a peristaltic pump, providing a cost-effective and industrially feasible route for clinical translation. Overall, this work represents not only a formulation development and optimization phase, where combined *in vitro* characterization and *ex vivo* skin permeation studies provide key insights into nanocarrier performance and skin delivery, but also a systematic and scalable framework for the rational design of complex nanocarrier systems.

2. Materials and methods

2.1. Materials

18*β*-Glycyrrhetinic acid (18*β*-GA) was purchased from Sharon Personal Care (Milan, Italy), Lipoid® S100 (S100, soybean lecithin, 94% of phosphatidylcholine) was kindly provided by Lipoid GmbH (Ludwigshafen, Germany), vegetable glycerol was purchased from Farmalabor (Barletta, Italy), SAFIC' Care T A 500 (Alginate) was kindly provided by Safic Alcan (Milan, Italy), Creamelt® COC (Cyclic Olefin Copolymer) 3D printing filament was purchased from Creamelt (Rapperswil-Jona, Switzerland), absolute ethanol (EtOH $\geq$ 99,8%) was purchased from Sigma-Aldrich (St. Louis, MO, USA). High-performance liquid chromatography (HPLC) grade methanol (MeOH) was acquired from VWR (Leuven, Belgium). Purified water was sourced from a Millipore Milli-Q Ultrapure water purification system (Millipore, Bedford, MA, USA).

2.2. 3D printing of COC microfluidic chips

The 3D printed microfluidic chip was designed using computer-aided design (CAD) software, allowing for the optimization of the internal architecture to promote efficient passive micromixing. The internal geometry features a three-dimensional flow-focusing junction, in which the central sample stream is hydrodynamically confined by converging lateral streams under laminar co-flow conditions, enhancing interfacial area and promoting diffusion-driven mixing. Ultimaker Cura 4.3 software (Ultimaker, Utrecht, Netherlands) was used to convert it for printing. The device was fabricated using a FDM 3D printer (Ultimaker 3, The Netherlands) with Cyclic Olefin Copolymer filament. Printing was performed at a speed of 25 mm/s, using a 0.25 mm nozzle at a temperature of 240 °C. In the final setup, probe needles and polyethylene tubing were used to connect the 3D-printed chip to two syringes mounted on syringe pumps (Aladdin, WPI Europe, Friedberg, Germany).

2.3. Microfluidic formulation of ethosomes, glycethosomes and glycerosomes

For the preparation of nanocarriers by microfluidics, a defined amount of S100 and 18*β*-GA, or S100, 18*β*-GA, and glycerol, was dissolved in absolute ethanol and pumped against water or a mixture of water and glycerol at controlled flow rates, using different flow rate ratios (FRR), in order to maintain a final ethanol concentration of 25% *v*/v. Glycerol was equally divided between the water and ethanolic phases, taking into account the required final concentration in the formulation. The samples were collected from the chip's outlet. For glycerosomes, the organic solvent was evaporated under vacuum using a sample concentrator (Alltech Model 190 A, Alltech Inc., United States) (Fig. 1). The specific experimental conditions used for the preparation of all nanocarriers were defined according to the DoE.

2.4. Design of experiments (DoE)

The DoE consisted of a Screening Design followed by an Optimization Design, performed using Design Expert Stat-Ease® software (v. 23.1) (Stat-Ease Inc., USA). This approach was used to evaluate the main effects of the process parameters (independent variables) such as S100 concentration, 18*β*-GA concentration, total flow rate (TFR), and glycerol concentration, as well as their interactions on the particle size and PDI (dependent variables), by applying a two-level full factorial design for the screening (Montgomery, 2017) and a central composite design (CCD) and a Box-Behnken Design (BDD) for the optimization. ANOVA analysis was carried out to define and validate the multiple regression mathematical model. Each experimental condition was tested in triplicate, using a randomized block design with three blocks to account for systematic variability. A significance level of 5% ($p < 0.05$) was adopted for statistical evaluation. The regression performance was assessed using

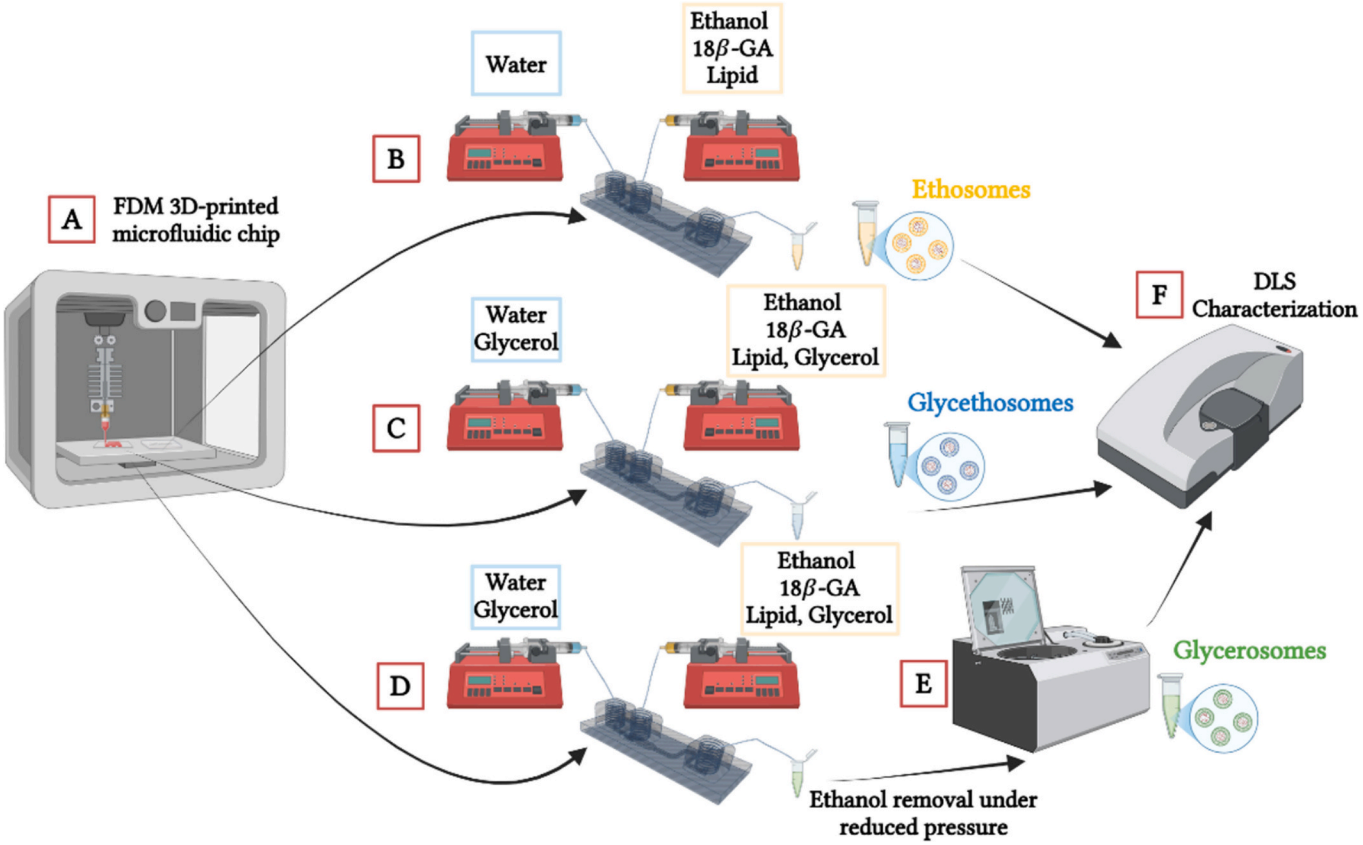

Fig. 1. Fabrication of the 3D-printed microfluidic chip (A); microfluidic production of Ethosomes (B), Glycethosomes (C), and Glycerosomes (D); ethanol removal (E); DLS characterization (F).Printing of 3D-printed chip (A); Ethosomes production with microfluidic chip (B); Glycethosomes production (C); Glycerosomes production (D); Ethanol removal (E); Characterization with DLS (F).

the coefficients of determination: R^2, adjusted R^2 (adj-R^2), and predicted R^2 (pred-R^2). The R^2 value is usually used to indicate how well the model fits the experimental data, but it tends to increase with the addition of new variables, regardless of their actual relevance, potentially leading to overfitting. In contrast, the adjusted R^2 is more accurate, accounts for the number of predictors in the model and increases only when the new term significantly improves the model's performance. This allowing a more reliable comparison between models with different complexities. The predicted R^2 evaluates the model's ability to predict new data. A good agreement between adj-R^2 and pred-R^2 (difference lower than 0.2) suggests that the model has both a good fit and strong predictive capability.

2.4.1. Screening design

A two-level full factorial design (2^3) was used to evaluate the process factors' effects for ethosomes (S100 concentration, 18β-GA concentration, TFR); while a two-level full factorial design (2^4) was used to evaluate the process factors' effects for glycethosomes and glycerosomes (S100 concentration, 18β-GA concentration, TFR, and glycerol concentration). The actual and coded values for each factor are summarized in Table S1, particle size and PDI were considered as response variables. To improve the model's accuracy and estimate experimental variability, the design was divided into three blocks, and three central points were added. This resulted in a total of 27 experimental runs for ethosomes (Table S2) and 51 experimental runs each for glycethosomes (Table S3) and glycerosomes (Table S4).

2.4.2. Optimization design

To perform the optimization, different designs were employed according to the number of factors investigated. A Central Composite Design was used for ethosomes, as only two independent variables were considered (S100 concentration and TFR), while a Box-Behnken Design was used for glycethosomes and glycerosomes, where three factors were evaluated (S100 concentration, TFR, and glycerol concentration). Based on the results obtained in the screening design, the range for each factor was defined, while the 18β-GA concentration was fixed at 0.5 mg/mL. The actual and coded values for each factor are summarized in Table 1, particle size and PDI were considered as response variables.

2.5. Physicochemical characterization of nanocarriers

2.5.1. Dynamic light scattering (DLS)

Dynamic light scattering (DLS, Zetasizer Nano S Instrument Ltd., Malvern Panalytical Srl, Worcester, UK) was used to characterize the prepared formulations in term of average particle size (*Z*-average) and PDI. Samples were diluted in purified deionized water (1:100 *v*/v), measurements were performed at 25 °C, and all the experiments were performed in triplicate. The results are expressed as the mean ± standard deviation.

Table 1
Actual and coded values of the selected factors for the optimization design.

	Coded Value		
	−1	0	+1
	Actual Value		
S100 concentration (mg/mL)	6	8	10
TFR (mL/min)	20	30	40
Glycerol concentration (% v/v)	10	30	50

2.5.2. Drug encapsulation efficiency (EE%) studies

Encapsulation efficiency (EE%) studies of the optimized formulations were carried out using an indirect method. First, samples were diluted in deionized water 1:6 and ultracentrifuged at 45000 rpm and 4 °C for 60 min, then the amount of unloaded 18β-GA was measured in the supernatant using HPLC (Agilent 1260 Infinity II, Agilent Technologies, Santa Clara, CA, USA) equipped with a C18 column (InfinityLab Poroshell 120 C18 column, 3 × 100 mm, Agilent Technologies, Santa Clara, CA, USA), with an isocratic mixture of 0.5% formic acid in deionized water and methanol (ratio 15:85 *v*/v) as mobile phases, with a flow rate of 1 mL/min. The injection volume was 20 µL and the detection signal was recorded at 254 nm (UV lamp) keeping the analysis system at room temperature. Before the analyses, a calibration curve of 18β-GA standard was prepared with several concentrations in the range of 0.001 to 0.25 mg/mL with a correlation coefficient (R^2) of 0.9967 for ethosomes, 0.9985 for glycethosomes and 0.9995 for glycerosomes. The limit of detections and the limit of quantification were 0.019 µg/mL and 0.057 µg/mL respectively. All the experiments were performed in triplicate. The results are expressed as the mean ± standard deviation. The EE% of 18β-GA was calculated with the following equation (Eq. (1)):

$$EE\% = \frac{T_{drug} - S_{drug}}{T_{drug}} X\,100 \quad (1)$$

where T_{drug} is the total amount of drug used for the formulation and S_{drug} is the amount of drug in the supernatant measured with HPLC.

2.5.3. Nanoparticle tracking analysis (NTA) and ζ-potential

Nanoparticle tracking analysis (NTA) *and* ζ-potential measurements of the optimized formulations were performed using a NanoSight LM10 instrument (Malvern Panalytical Srl, Worcester, UK). Before the test, the samples were serially diluted with distilled water to reach a particle concentration suitable for analysis with NTA and injected into the LM unit using a 1 mL sterile syringe. Five 60-s videos were recorded and then analyzed using NTA 3.1 analytical software (NanoSight, Malvern, UK). All the experiments were performed in triplicate. The results are expressed as the mean ± standard deviation.

2.5.4. Transmission electron microscopy (TEM)

The optimized formulations were also characterized by transmission electron microscopy (TEM, HT 7800 series, Hitachi, Tokyo, Japan), using an acceleration voltage of 100 kV to confirm the vesicle formation and evaluate the morphology. Before the analyses, samples were stained with phosphotungstic acid solution (1%). Briefly, a droplet of nanoparticle suspension was deposited on a formvar-carbon-coated copper grid and then, dried the excess using a filter paper. Subsequently a droplet of 1% phosphotungstic acid solution was added to the grid to obtain a negative staining. After removing the excess of liquid, the grid was washed with two droplets of water and air dried at room temperature.

2.6. Stability studies

The stability of the optimized nanocarrier formulations was assessed by storing them at 4 °C for 3 months and analyzing them periodically (0, 7, 14, 21, 30, 60, 90 days). All the formulations were evaluated for particle size, PDI, EE%, NTA and ζ-potential. All the experiments were performed in triplicate, and the results are expressed as the mean ± standard deviation.

2.7. Gel preparation and characterization

The optimized formulations were selected to prepare hydrogels for topical application, using alginate as a gelling agent. Alginate is a natural anionic polysaccharide composed primarily of β-D-mannuronic acid and α-L-guluronic acid residues, which forms viscous gels upon hydration (Abka-khajouei et al., 2022). Briefly, 0.4% *w/v* alginate was slowly added to the vesicle suspensions containing 0.5% (*w/v*) of 18β-GA under continuous stirring (300 rpm) at room temperature. The mixtures were stirred until the polymer was fully hydrated and a homogeneous hydrogel was formed. This concentration was selected based on preliminary tests to achieve a viscosity suitable for topical application, ensuring ease of spreading and adequate skin adhesion. The hydrogels were characterized for pH and rheological properties using a rheometer (MCR302e, Anton Paar, Graz, Austria) equipped with a plate-plate geometry (PP, 25 mm Ø, gap 1 mm). Flow curves were acquired using a shear rate ramp from 0.1 to 100 s^{-1} at 25 °C, while Amplitude sweep tests were conducted at a fixed frequency of 1 Hz, with strain values ranging from 0.01% to 1000% at 25 °C.

2.8. Ex vivo permeation studies using Franz-type diffusion cells

2.8.1. Skin preparation

Porcine skin was used in this study due to its similar morphology to human skin (Summerfield et al., 2015). Fresh porcine skin obtained from the Department of Veterinary and Animal Sciences (University of Copenhagen) was cleaned with PBS (pH 7.4 at 25 °C), skin sections were cut out, and the hair was trimmed. The sections were subsequently dermatomed using a Zimmer Dermatome AN (Zimmer Biomet Denmark, Albertslund, Denmark) to achieve a thickness of 500 µm. The dermatomed skin was then stored at −20 °C until further use.

2.8.2. Skin permeation and retention studies

The skin was mounted on vertical Franz diffusion cells (Phoenix DB-6 Dry Heat Diffusion Cells, Teledyne Hanson Research, Chatsworth, CA, USA) with a diffusional surface area of 1 cm^2. 10 mL of EtOH:PBS mixture (30:70 *v*/v) was used as the receptor solution, which was continuously agitated throughout the course of the experiments (600 rpm). Addition of EtOH ensured sufficient solubility of the drug in the receptor medium (Tiboni et al., 2020). The system was thermostatted at 35 °C ± 0.1 °C to provide a skin surface temperature of 32 °C ± 0.1 °C (Oh et al., 2020). Before testing, the receptor solution was degassed by ultrasonic treatment for 30 min. Dermatomed skin sections were thawed, fixed on the Franz cells with the epidermal side facing up, left to equilibrate for approximately 30 min. To confirm skin integrity, transepidermal water loss (TEWL) was measured using an AquaFlux™ AF200 probe (Biox Systems Limited, London, UK) equipped with a coupling element, enabling direct measurements from the donor chamber of the Franz cells. Skin with TEWL < 20 $g/m^2/h$ is widely accepted as indicative of an intact SC barrier, considered intact and included in the experiments (OECD, 2004; Levin and Maibach, 2005; Fluhr et al., 2006). The measurements were taken prior to and after the permeation studies, and at least three measurements were taken for each of the skin pieces. By testing the solubility of 18β-GA in the receptor media beforehand, we ensured that sink conditions were met. 740 µL of the formulation containing 0.5% 18β-GA was applied on the skin (Summerfield et al., 2015). At specific time points (19, 20, 21, 22, 23, and 24 h) aliquots of 600 µL were withdrawn from the receptor chambers, replenished with fresh receptor solution and centrifuged (21,130 ×*g*, 20 min). Supernatants were collected, and the content of 18β-GA was determined using HPLC. A 24 h experimental timeframe was selected in accordance with standard Franz diffusion cell protocols for topical formulations, representing a widely used endpoint for evaluating short-term skin permeation and retention profiles under controlled *ex vivo* conditions.

The cumulative amount of 18β-GA permeated through the skin at time *t* (Q_t) was determined using the equation (Eq. (2)) (Fda and Cder, 2026):

$$Q_t = \frac{C_t V_R + \left(\sum_{i=1}^{t-1} C_i\right) V_s}{A} \quad (2)$$

where: C_t (mg/mL) is the concentration of 18β-GA in the aliquot

collected at time t, V_R (mL) is the volume of the receptor solution, $\sum_{i=1}^{t-1} C_i$ is the sum of 18β-GA concentrations in the aliquots at times from i to t-1, V_S is the volume of the aliquots, A is the permeation area (1 cm^2).

The percentage of cumulative amount of 18β-GA permeated over time was calculated by the following equation (Eq. (3)) (Coderch et al., 2021):

$$Q\% = \frac{Q_t}{Total\ amount\ of\ 18\beta GA\ applied} X\ 100 \quad (3)$$

After 24 h any liquid present in the donor chambers was collected and residual formulation remaining on the epidermal surface of the skin was removed with cotton swabs. The samples were left for 30 min to ensure a dry environment inside the chambers. Afterwards, the impact of the formulations on the skin integrity was assessed by measuring changes in its TEWL. For amounts of unpermeated 18β-GA in the retained formulation, the swabs were transferred into 5 mL Eppendorf tubes, and 1 mL of the extraction solvent (MeOH) was added. For drug retention analysis, the Franz cells were disassembled, and the skin sections were then wrapped in aluminium foil, heated at 60 °C in an oven for 15 min, and then separated into epidermis and dermis using a scalpel and tweezers. Each separated skin layer was placed into a 5 mL Eppendorf tube, and 1 mL of the extraction solvent (MeOH) was added. All the tubes were sonicated (20 min), vortex-mixed and left at room temperature for 24 h under gentle agitation. Finally, the extractants were centrifuged (21,130 ×g, 20 min), supernatants were collected, and the content of 18β-GA in the samples was determined by HPLC as described above.

2.9. Scalability studies

Scalability studies were conducted to assess if nanoparticle production could be increased while maintaining the physicochemical properties previously optimized at laboratory scale. To produce larger volumes, the syringe pump was replaced with a peristaltic pump, while keeping the microfluidic chip design and the critical formulation parameters unchanged, including ethanol, glycerol, S100, and 18β-GA concentrations. As the peristaltic pump could not reach the same TFR as the syringe pump, the flow rates were set to the maximum achievable, keeping the FRR constant to maintain the final formulation composition. For glycerosomes, the organic solvent was evaporated on a heating stirrer at 50 °C overnight, as the sample concentrator used at small scale was not suitable for larger volumes. The effect of scale-up on nanoparticle quality was evaluated by comparing the larger-scale batches with the laboratory-scale reference formulations in terms of particle size and polydispersity index (PDI).

2.10. Statistical analysis

Data analysis was performed using OriginPro software (version 2022) (OriginLab Corporation, Northampton, MA, USA) For the DoE, an Analysis of Variance ANOVA was performed to identify significant factors at a 5% significance level. Model quality was assessed using p-values, F-values, and regression coefficients R^2, adj-R^2 and pred-R^2. Models were considered significant when $p < 0.05$, and the best-fitting model for each response was selected based on the highest adj-R^2 and a difference between pred-R^2 and adj-R^2 below 0.2. Coded equations were used to identify influential factors and interactions, while equations based on actual factor levels were used to generate response surface plots. For the skin integrity testing, a two-way ANOVA followed by Tukey's multiple comparison test was employed to determine the statistical differences between the groups. The differences in skin retention between the groups were determined with a one-way ANOVA followed by Tukey's multiple comparison test. Results are presented as means with their standard deviations, and statistical significance is indicated by p-values as follows: (*) for $p \leq 0.05$, (**) for $p \leq 0.01$, (***) for $p \leq 0.001$, (****) for $p \leq 0.0001$. 3D plots were created using OriginPro software.

3. Results and discussion

3.1. Fabrication and performance of the 3D-printed microfluidic chip

Nanocarriers were produced using a customized 3D-printed microfluidic chip, enabling precise control over particle size and PDI through passive micromixing. The chip design promoted efficient laminar coflow between the aqueous and ethanolic phases, which entered through separate inlets and converged in the micromixing region before collection. This configuration ensured rapid, homogeneous mixing, facilitating controlled nucleation and growth of lipid vesicles. Microfluidics offers advantages over conventional methods, as laminar flow at the microscale enables predictable mixing, uniform particle formation, and minimal batch to batch variability, while supporting high drug loading efficiency. Coupled with fused deposition modeling (FDM), this approach provides a low-cost, accessible, and scalable platform for producing nanocarriers with tight control over critical quality attributes (Tiboni et al., 2021; Zhang et al., 2023).

3.2. Screening of the nanocarriers manufacturing process by microfluidics

A 2-Level Full Factorial Design was adopted to evaluate the main effects of the independent variables, S100 concentration (X_1), TFR (X_2), 18β-GA concentration (X_3), and glycerol concentration (X_4), as well as their interactions, on dependent variables, particle size (Y_1) and PDI (Y_2). The coded equations and the FIT statistics parameters are reported in Table S5 and Fig. S1. Based on the coefficients of the coded equation, the particle size of ethosomes increased with increasing S100 concentration and decreasing TFR. In contrast, the particle size of glycethosomes and glycerosomes increased with decreasing S100, 18β-GA concentration and glycerol concentration and increasing TFR. Ethosomes PDI decreased with increasing S100 concentration, TFR and 18β-GA concentration, glycethosomes PDI decreased with increasing S100 concentration, TFR, 18β-GA concentration and glycerol concentration, while for glycerosomes, PDI decreased with increasing S100 concentration and TFR, and decreasing 18β-GA and glycerol concentration. Based on the analysis, manufacturing conditions to produce the smallest and largest average size and PDI were selected for the subsequent study. We proceeded with the optimization process focusing on the variables X_1 (S100 concentration), X_2 (TFR), and X_4 (glycerol concentration), while fixing X_3 (18β-GA concentration) at 0.5 mg/mL. Although X_3 is a significant parameter in some of the equations, it was excluded from the variable set to ensure comparability of the results. This drug concentration represents the highest value that can be successfully encapsulated while maintaining an acceptable PDI for the nanoparticles, as also confirmed by a previous study reported by Tiboni et al. (Tiboni et al., 2020).

3.3. Optimization of the nanocarriers manufacturing process by microfluidics

The selected optimization area for the process was defined within a S100 concentration range from 6 to 10 mg/mL, a TFR range from 20 to 40 mL/min, and a glycerol concentration from 10 to 50% (v/v) (for glycethosomes and glycerosomes), with a fixed 18β-GA concentration at 0.5 mg/mL. A Central Composite Design (CCD) was applied for ethosomes (Table 2) and a Box–Behnken Design (BBD) for glycethosomes (Table 3) and glycerosomes (Table 4). The central points were analyzed in triplicate to improve the reliability of the results, for a total of 11 experiments for ethosomes and 15 for glycethosomes and glycerosomes. The responses observed were first fitted to the quadratic mathematical model and then refined by eliminating the insignificant terms of equations (whose p-value >0.05), as summarized in Table 5. Across all the

Table 2
Optimization of the microfluidic manufacturing process of ethosomes by DoE: size and PDI of the different runs.

Standard	Run	Input		Output	
		X_1	X_2	Y_1	Y_2
		S100 concentration (mg/mL)	TFR (mL/min)	Particle size (nm)	PDI
4	1	10	40	109 ± 2	0.23 ± 0.01
1	2	6	20	94 ± 2	0.23 ± 0.02
2	3	10	20	144 ± 5	0.33 ± 0.03
6	4	10	30	122 ± 1	0.26 ± 0.01
11	5	8	30	101 ± 2	0.23 ± 0.01
3	6	6	40	74 ± 1	0.21 ± 0.01
9	7	8	30	98 ± 2	0.22 ± 0.02
5	8	6	30	98 ± 14	0.23 ± 0.05
10	9	8	30	95 ± 1	0.20 ± 0.02
7	10	8	20	110 ± 1	0.23 ± 0.01
8	11	8	40	90 ± 1	0.22 ± 0.01

screening designs, the refined model exhibited a significantly lower p-value and a higher adj-R^2 compared to the quadratic model, indicating improved accuracy and reliability. Moreover, the pred-R^2 was in good agreement with the adj-R^2, as the difference between the two was lower than 0.2, for all of them except the refined mathematical model for the PDI (Y_2) of the ethosomes, where a negative pred-R^2 was obtained. This indicates limited predictive capability of the model for this specific response within the investigated experimental domain. Accordingly, this limitation does not affect the overall robustness of the DoE approach, as the optimization strategy was primarily driven by particle size as the main critical quality attribute, while PDI was considered a secondary descriptor, consistently remaining within acceptable limits across all formulations. Confirmation experiments were therefore essential to validate the selected optimal conditions and ensure model reliability within the defined design space.

Based on the coefficients of the coded equation (Table 5), the particle size of ethosomes and increased with increasing S100 concentration and decreasing TFR. Similarly, the particle size of glycethosomes increased with increasing S100 and glycerol concentration and decreasing TFR. In contrast, the particle size of glycerosomes increased with decreasing S100 and glycerol concentration and increasing TFR. Ethosomes PDI decreased as S100 concentration decreased and TFR increased. For glycethosomes, PDI decreased with lower S100 concentration and higher glycerol concentration, while for glycerosomes, PDI decreased when S100 concentration increased and glycerol concentration decreased. Fig. 2 shows the 3D response surface plots related to the correlations between particle size and PDI with TFR and S100 concentration for ethosomes (Fig. 2a–b, respectively) as well as the correlations between particle size and PDI with glycerol and S100 concentration for glycethosomes (Fig. 2c–d) and glycerosomes (Fig. 2e–f), respectively. The developed models were validated by comparing the predicted values for the selected formulation with the experimentally obtained results. The differences between the predicted and experimental values were within the acceptable range, thus confirming the predictive reliability of the model and supporting the robustness of the optimization strategy (Table S6).

3.4. Physicochemical characterization of optimized formulations

Based on the outcomes of the optimization study, three formulations were selected for further characterization. They were chosen based on their particle size within the desired nanometric range (70–100 nm), an acceptable PDI indicative of homogeneous size distribution, and fixed concentrations of glycerol (30% *v*/v) and 18*β*-GA (0.5 mg/mL), for ensuring consistency and comparability across nanocarrier systems. The formulations identified as optimal, one for ethosomes, one for glycethosomes, and one for glycerosomes, exhibited the best compromise between small particle size, low PDI, and appropriate excipient composition, as predicted by the refined DoE models and confirmed experimentally. These optimized nanocarriers were therefore selected for comprehensive physicochemical characterization and nanostructure assessment (Table 6).

3.4.1. Drug encapsulation efficiency (EE%), ζ-potential and stability studies

The optimized formulations were assessed through a long-term stability study by measuring particle size and PDI over multiple time points throughout the 90-day period, while EE and ζ-potential were determined at time 0 and at the end of storage. Together, these parameters provide a comprehensive indication of the structural integrity, colloidal behavior, and overall suitability of the vesicles for skin delivery (Danaei et al., 2018). The stability study confirmed the robustness of the optimized nanocarriers. Ethosomes maintained a narrow size range (77–92

Table 3
Optimization of the microfluidic manufacturing process of glycethosomes by DoE: size and PDI of the different runs.

Standard	Run	Input			Output	
		X_1	X_2	X_3	Y_1	Y_2
		S100 concentration (mg/mL)	TFR (mL/min)	Glycerol concentration (% v/v)	Particle size (nm)	PDI
11	1	8	20	50	125 ± 1	0.23 ± 0.01
1	2	6	20	30	85 ± 1	0.28 ± 0.02
9	3	8	20	10	94 ± 1	0.22 ± 0.01
3	4	6	40	30	64 ± 1	0.29 ± 0.01
10	5	8	40	10	82 ± 1	0.19 ± 0.01
8	6	10	30	50	161 ± 2	0.36 ± 0.01
12	7	8	40	50	130 ± 1	0.35 ± 0.01
13	8	8	30	30	80 ± 1	0.24 ± 0.01
4	9	10	40	30	100 ± 1	0.35 ± 0.01
7	10	6	30	50	121 ± 1	0.24 ± 0.01
6	11	10	30	10	149 ± 2	0.40 ± 0.01
2	12	10	20	30	116 ± 1	0.33 ± 0.01
14	13	8	30	30	110 ± 2	0.43 ± 0.01
15	14	8	30	30	79 ± 1	0.24 ± 0.01
5	15	6	30	10	73 ± 1	0.22 ± 0.01

Table 4
Optimization of the microfluidic manufacturing process of glycerosomes by DoE: size and PDI of the different runs.

Standard	Run	Input			Output	
		X_1	X_2	X_3	Y_1	Y_2
		S100 concentration (mg/mL)	TFR (mL/min)	Glycerol concentration (% v/v)	Particle size (nm)	PDI
2	1	10	20	30	117 ± 3	0.26 ± 0.01
3	2	6	40	30	97 ± 2	0.51 ± 0.04
13	3	8	30	30	98 ± 1	0.25 ± 0.01
14	4	8	30	30	96 ± 1	0.26 ± 0.01
10	5	8	40	10	90 ± 1	0.24 ± 0.01
4	6	10	40	30	95 ± 1	0.24 ± 0.01
11	7	8	20	50	147 ± 2	0.33 ± 0.01
12	8	8	40	50	175 ± 3	0.37 ± 0.01
7	9	6	30	50	220 ± 51	0.39 ± 0.02
8	10	10	30	50	188 ± 2	0.37 ± 0.02
9	11	8	20	10	101 ± 1	0.22 ± 0.01
5	12	6	30	10	84 ± 1	0.26 ± 0.01
1	13	6	20	30	100 ± 1	0.27 ± 0.01
6	14	10	30	10	107 ± 1	0.23 ± 0.01
15	15	8	30	30	96 ± 1	0.28 ± 0.02

Table 5
Analysis of variance (ANOVA) for particle size and PDI.

	R^2	Adj-R^2	Pred-R^2	Refined model (Coded equation)
	Particle size (Y_1)			
Ethosomes	0.8842	0.8346	0.6471	$Y_1 = 54471.63 + 32989.15\,X_1 - 31246.19\,X_2 + 29038.03X_{12}$
Glycethosomes	0.8929	0.8500	0.7992	$Y_1 = 90.44 + 18.4\,X_1 - 5.44\,X_2 + 21.75\,X_3 + 21.98\,X_3^2$
Glycerosomes	0.9559	0.9228	0.8167	$Y_1 = 0.000037 - 4x10^{-6}X_1 + 0.000003\,X_2 - 1.6x10^{-5}X_3 + 0.000006\,X_{13} - 4x10^{-6}X_{23} - 1.1x10^{-5}X_3^2$
	PDI (Y_2)			
Ethosomes	0.6852	0.5503	−0.2227	$Y_2 = 0.2355 + 0.0248\,X_1 - 0.0197\,X_2 - 0.0222\,X_{12}$
Glycethosomes	0.3165	0.2026	0.0880	$Y_2 = 0.2845 + 0.0372\,X_1 + 0.0339\,X_3$
Glycerosomes	0.5291	0.4507	0.2709	$Y_2 = 0.2984 - 0.0416\,X_1 + 0.0648\,X_3$

nm) throughout the 90-day period, showing only a slight increase, while PDIs remained low (0.18–0.27). Glycethosomes displayed a similarly stable profile, with vesicle size varying moderately from 73 to 93 nm and consistently low PDI values (0.18–0.22). Glycerosomes were found to be the most stable, maintaining a nearly unchanged nanoscale size (93–92 nm) and exhibiting a slightly higher initial PDI, which remained constant over time (0.27–0.28), indicating no signs of vesicle aggregation or structural destabilization. All formulations displayed satisfactory EE%, although with distinct trends consistent with their composition. Ethosomes showed the highest drug-loading capacity (above 81%), confirming the strong affinity of 18β-GA for ethanol-fluidized phospholipid bilayers. Glycethosomes and glycerosomes exhibited slightly lower values (above 69% and 63%, respectively), in line with their reduced ethanol content and the increased structuring effect of glycerol on the vesicle membrane. Importantly, no marked changes in EE% were observed at the end of the study, confirming the absence of drug leakage or vesicle destabilization. The ζ-potential values were negative for all systems, reflecting the anionic nature of phospholipid headgroups and the presence of ethanol and/or glycerol. Ethosomes showed the most negative values at time 0 (−24 mV), with a slight decrease to −17 mV after 90 days, whereas glycethosomes and glycerosomes displayed slightly less negative charges (−20 mV and − 17 mV, respectively) that remained stable over time. These values indicate good colloidal stability and are consistent with the formation of well-dispersed vesicular systems. Overall, these data demonstrate that all three optimized formulations exhibit high drug-loading capacity, appropriate surface charge, and excellent physicochemical stability over time, thereby supporting their suitability for subsequent skin-delivery analysis (Table 7). Fig. 3 shows TEM analysis of the optimized nanoparticles, confirming the formation of nanosized vesicles. All nanoparticles were uniform, smooth, and regularly spherical, with a homogeneous dispersion. In glycethosomes and glycerosomes, a layer of glycerol surrounding the vesicles was observed, leading to a close-packed arrangement and the formation of a three-dimensional network, as previously reported by Manca et al. (Manca et al., 2019).

3.5. Physicochemical and rheological properties of hydrogels

The optimized formulations were formulated into alginate-based hydrogels (0.4% *w/v*) to enable topical application and improve patient compliance. Further studies were performed to complement the physicochemical characterization and to assess the rheological properties of the hydrogels. Fig. 4 report the shear stress *vs* shear rate and shear viscosity *vs* shear rate curves. The shear stress/shear rate curves were fitted with the Herschel-Bulkley model (Eq. (4)), where the τ_0 is the yield stress, K (Pa s^n) is the consistency index and *n* is the flow behavior index. When $n = 1$, the fluid has a Newtonian behavior, or it is a Bingham fluid if τ_0 is greater than zero. For $n < 1$ the fluid exhibits shear-thinning behavior. Smaller values of n indicate stronger shear thinning, with the effect becoming increasingly pronounced as n approaches zero. On the other hand, for $n > 1$, the fluid exhibits shear-thickening behavior.

$$\tau = \tau_0 + K\gamma^n \quad (4)$$

As expected, (Table S7) for the glycethosomes and glycerosomes, the suspensions showed a Newtonian behavior with n approaching to 1; while the hydrogels showed a shear thinning behavior (n < 1). The ethosomes showed a shear thinning behavior in both suspensions and hydrogel formulations. Moreover, as expected, all the hydrogels showed a consistency index higher than the suspensions.

3.6. Skin studies

Once physicochemical and morphological stability had been verified, the optimized nanocarriers were evaluated for their skin-delivery

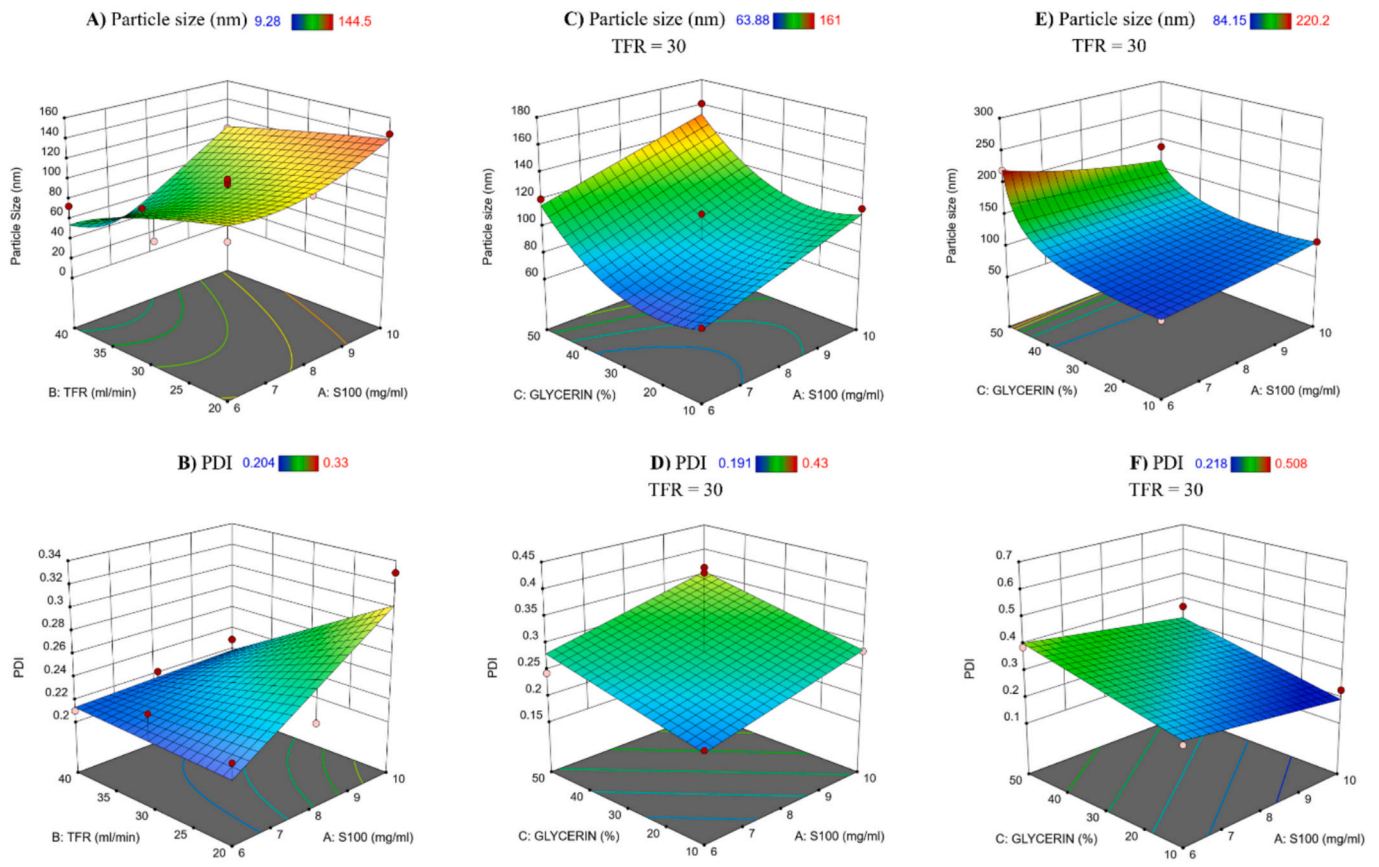

Fig. 2. Optimization Design space revealed the correlation between the process parameters and samples morphology. Particle size of ethosomes (A); PDI of ethosomes (B); Particle size of glycethosomes (C); PDI of glycethosomes (D); Particle size of glycerosomes (E); PDI of glycerosomes (F).

Table 6
Selected formulation parameters.

	S100 (mg/mL)	TFR (mL/min)	GA (mg/mL)	Glycerol (% v/v)	Particle Size (nm)	PDI
Ethosomes	6	30	0.5	/	78 ± 1	0.18 ± 0.02
Glycethosomes	6	30	0.5	30	73 ± 1	0.18 ± 0.04
Glycerosomes	10	40	0.5	30	93 ± 12	0.27 ± 0.04

performance through *ex vivo* permeation and retention studies. The experiments aimed to determine whether differences in vesicle composition, particularly the presence of ethanol or glycerol, translated into distinct permeation and retention profiles. For this purpose, porcine skin was used as a biological membrane in a Franz diffusion cell setup.

3.6.1. Skin integrity testing

To evaluate the impact of 18β-GA-loaded nanocarriers on skin barrier integrity, the transepidermal water loss (TEWL) of the skin samples was measured before (0 h) and after 24 h of treatment with the assessed permeation-enhancing strategies (Fig. S2). Prior to treatment, all skin samples exhibited TEWL values below 20 g/m^2/h, confirming that they met EMA requirements for pre-experimental integrity assessment and ensuring that subsequent variations can be attributed solely to the applied formulations (Neupane et al., 2020; E. Medicines Agency, 2014). TEWL values for all formulations remained below 20 g/m^2/h after 24 h, indicating that the transient rise induced by ethanol-containing vesicles did not reach levels associated with barrier impairment. This observation is consistent with previous evidence showing that ethanol can fluidize and disorder stratum corneum lipids, enhancing their mobility and extractability without causing irreversible disruption (Gupta et al., 2020b).

3.6.2. Skin permeation and retention studies

The impact of 18β-GA nanocarriers on the skin permeation (Fig. S3) and retention is summarized in Fig. 5. After 24 h, the skin was separated into epidermis and dermis to more precisely assess drug retention. "Acceptor" indicates the proportion of 18β-GA that permeated through the skin into the acceptor compartment, whereas "Residue" indicates the proportion remaining in the drug delivery system after 24 h. The tested systems included ethosomes, glycethosomes, and glycerosomes, along with their corresponding hydrogel formulations. Two saturated solutions served as controls: Control 1 (18β-GA saturated solution in 25% *v*/v of ethanol in water) and Control 2 (18β-GA saturated solution in 25% v/v of ethanol +30% v/v glycerol in water). For glycethosomes, the highest percentage of 18β-GA remained in the donor phase, with 89.9 ± 1.7% remaining after 24 h, compared to 78.0 ± 6.3% for ethosomes and 70.3 ± 6.6% for glycerosomes. Correspondingly, 18β-GA levels in the epidermis and dermis were lower for glycethosomes (2.7 ± 0.5% and 2.8 ± 0.3% respectively) compared to ethosomes (10.2 ± 5.2% and 5.2 ± 2.0%) and glycerosomes (10.2 ± 3.2% and 4.1 ± 0.7%). Permeation into the acceptor compartment was minimal across all vesicular systems (glycethosomes 0.4 ± 0.1%, ethosomes 0.7 ± 0.6% and glycerosomes 0.2 ± 0.1%), with no statistically significant differences. Hydrogel formulations exhibited lower release and reduced skin uptake compared to the corresponding nanoparticle suspension, suggesting that the

Table 7
Stability studies, EE and ζ-potential. Data are reported as the mean of three independent replicates ± SD.

Day	Ethosomes				Glycethosomes				Glycerosomes			
	Size (nm)	PDI	EE%	ζ-potential (mV)	Size (nm)	PDI	EE%	ζ-potential (mV)	Size (nm)	PDI	EE%	ζ-potential (mV)
0	77 ± 1	0.18 ± 0.02	80.7 ± 3.9	−24.2 ± 1.2	73 ± 1	0.18 ± 0.04	63.0 ± 2.3	−20.0 ± 4.2	93 ± 12	0.27 ± 0.04	65.8 ± 8.7	−17.3 ± 3.2
7	77 ± 1	0.18 ± 0.03	–	–	71 ± 12	0.18 ± 0.04	–	–	92 ± 15	0.27 ± 0.01	–	–
14	81 ± 1	0.22 ± 0.01	–	–	74 ± 9	0.20 ± 0.01	–	–	106 ± 1	0.31 ± 0.10	–	–
21	80 ± 1	0.19 ± 0.01	–	–	89 ± 6	0.21 ± 0.01	–	–	90 ± 13	0.26 ± 0.01	–	–
30	82 ± 1	0.21 ± 0.01	–	–	88 ± 4	0.22 ± 0.03	–	–	90 ± 15	0.25 ± 0.01	–	–
60	87 ± 2	0.22 ± 0.01	–	–	95 ± 7	0.21 ± 0.03	–	–	91 ± 12	0.26 ± 0.01	–	–
90	92 ± 3	0.27 ± 0.03	81.5 ± 2.9	-16.9 ± 1.2	93 ± 3	0.22 ± 0.02	69.0 ± 3.8	−20.6 ± 4.6	92 ± 14	0.28 ± 0.01	63.3 ± 2.3	−17.8 ± 2.3

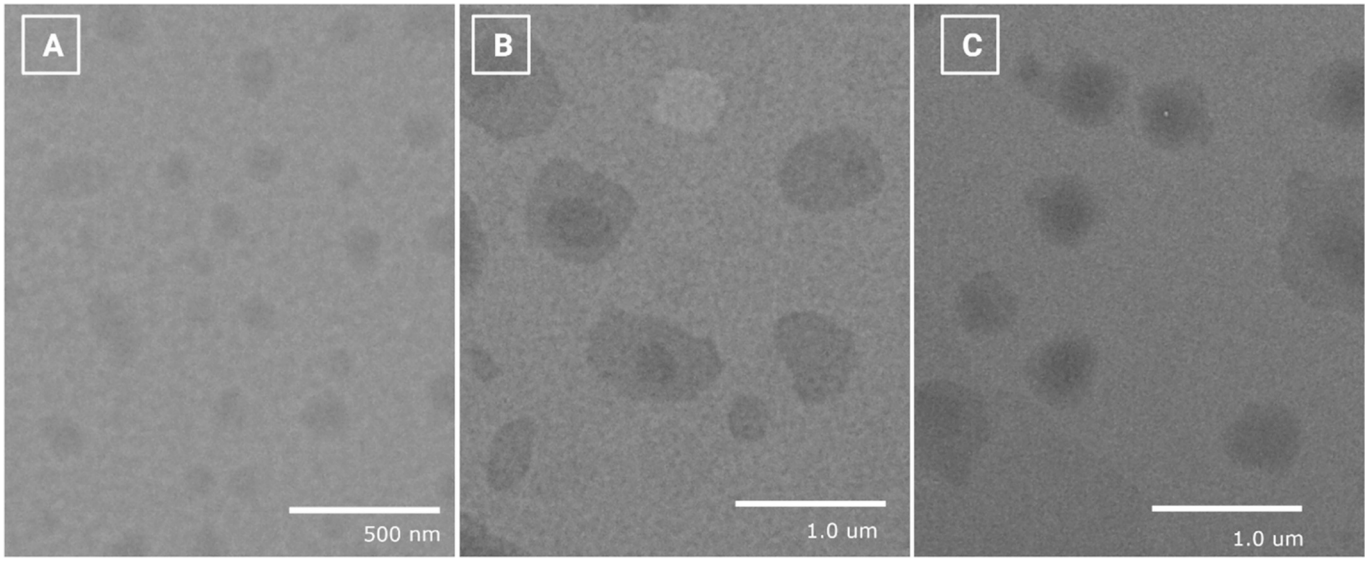

Fig. 3. Transmission electron microscopy (TEM) images of Ethosomes (A), Glycethosomes (B), and Glycerosomes (C).

polymeric matrix introduces an additional diffusional barrier that limits drug availability at the skin interface (Grijalvo et al., 2016). However, for practical topical delivery, hydrogel formulations are advantageous as they adhere better to the skin, improving contact time and ensuring more uniform application compared to liquid nanoparticle suspensions, consistent with the observed rheological behavior. Control 1 and 2 displayed higher drug levels in the skin, likely due to the steep concentration gradient generated by saturated solutions and the absence of carrier-mediated release constraints, resulting in rapid diffusion. These findings indicate that drug release from the formulation represents the rate-limiting step governing skin delivery, particularly for glycethosomes and hydrogel systems. The nanocarriers therefore act as formulation-based reservoir systems, modulating drug availability at the skin surface and supporting controlled and localized delivery (Manca et al., 2013; Peralta et al., 2018). The differences among the tested formulations can be attributed to specific interactions between glycerol, ethanol, and phospholipids. Glycethosomes (30% glycerol, 25% ethanol) exhibit increased bilayer rigidity due to glycerol hydrogen bonding with phospholipid headgroups, enhancing local microviscosity and stabilizing the membrane (Manca et al., 2013; Abou-Saleh et al., 2019). Although ethanol typically fluidizes lipid membranes, its effect is partially attenuated by glycerol, which competes for hydrogen bonding sites (Chanda et al., 2006). This results in more stable, less permeable membranes and reduced 18β-GA release. Glycerosomes, containing glycerol without ethanol, provide improved superficial skin permeation due to SC hydration while retaining vesicle deformability, whereas ethosomes achieve good 18β-GA penetration, being fluid and highly deformable (Zhang et al., 2022). Overall, glycethosomes are highly stable but exhibit reduced skin penetration, whereas glycerosomes combine high physicochemical stability with enhanced skin retention, making them the most suitable carrier for localized delivery of 18β-GA. Their ethanol-free composition further reduces the risk of irritation, supporting repeated topical application and sustained drug deposition in the skin.

3.7. Scalability studies

The scale-up was performed by continuously collecting the output from the microfluidic chip at regular intervals (0, 10, 20, 30, and 40 min), followed by analysis of particle size and PDI (Table 8). The TFR achieved for ethosomes was 23.5 mL/min, for glycethosomes 25.5 mL/min, and for glycerosomes 29.2 mL/min. Particle size and PDI values were in good agreement with the predicted values from the optimized DoE. Differences between predicted and observed values were within the acceptable range, further confirming the predictive reliability of the model and supporting the robustness of the optimization strategy.

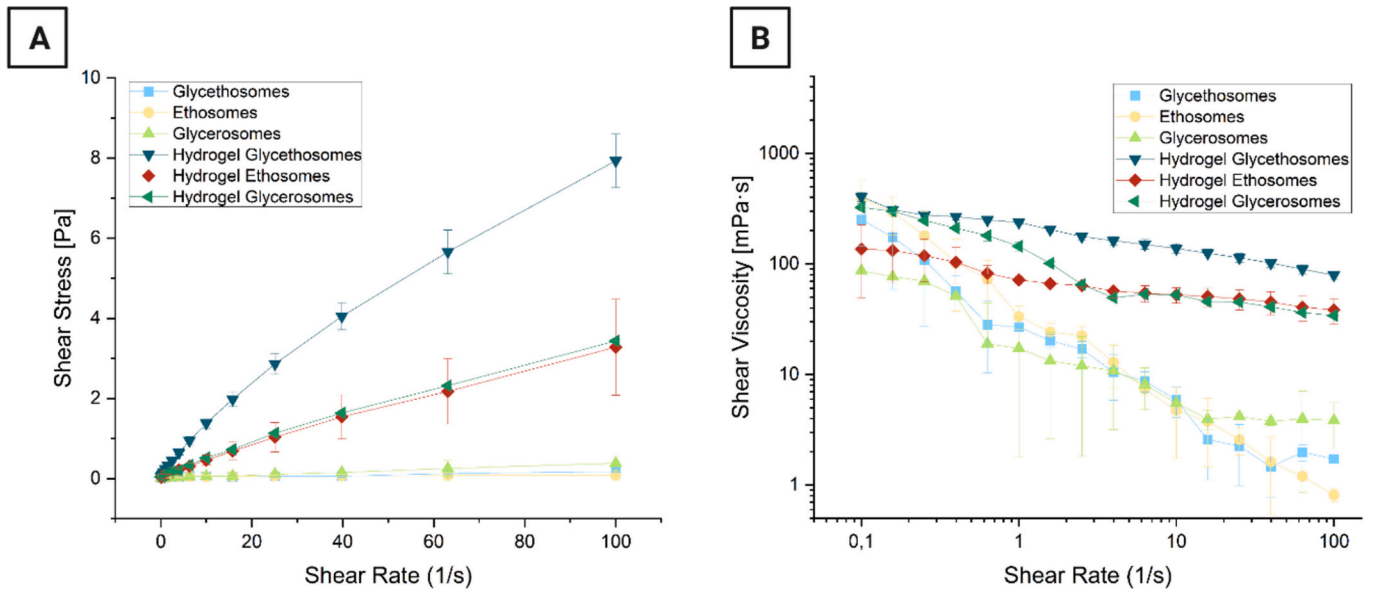

Fig. 4. Shear stress as a function of shear rate of nanoparticles formulations (A); Shear viscosity as a function of the shear rate of nanoparticles formulations (B). Data are reported as mean ± SD (n = 3).

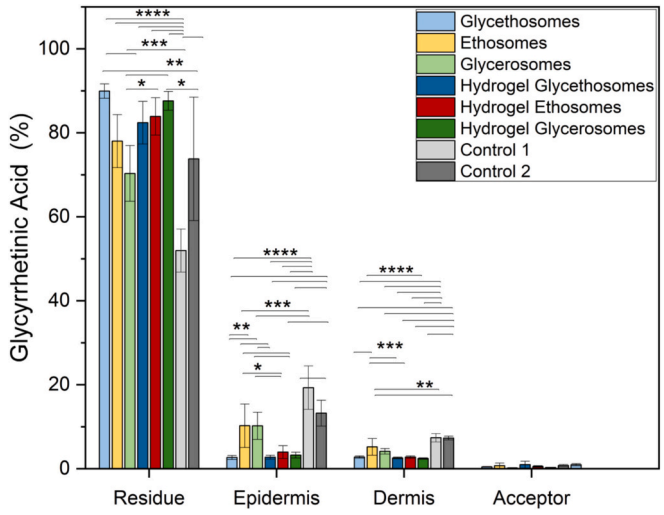

Fig. 5. Skin retention and permeation of 18β-GA. The 'Epidermis' and 'Dermis' bars represent the amount of 18β-GA retained in the respective skin layers, the "Residue" bar indicates the amount of 18β-GA remaining in the donor chamber after 24 h, while the 'Acceptor' bar indicates the amount permeated through the skin after 24 h. Data are reported as the mean of 6 replicates ± SD.

Reducing the TFR compared to laboratory-scale conditions led to only slightly increased of particle size and PDI, which nevertheless remained within acceptable limits for topical administration. The results also confirmed the stability of the production process over time: both the particle size and PDI remained relatively constant throughout the collection period, indicating reproducible and well-controlled nanoparticle formation. These findings demonstrate that the 3D-printed microfluidic chip, combined with the peristaltic pump, allows for continuous production of 18β-GA-loaded nanocarriers without compromising critical quality attributes. Overall, the process proved robust and scalable, supporting its potential application for larger batch manufacturing under controlled and reproducible conditions.

Table 8
Particle size and PDI of 18β-GA-loaded nanoparticles collected at different timepoint during the scale-up. Data are reported as the mean of three independent replication of experiments ± SD.

Time (minutes)	Ethosomes		Glycethosomes		Glycerosomes	
	Size (nm)	PDI	Size (nm)	PDI	Size (nm)	PDI
0	90 ± 1	0.20 ± 0.01	81 ± 1	0.29 ± 0.03	115 ± 2	0.37 ± 0.01
10	97 ± 1	0.25 ± 0.02	86 ± 2	0.31 ± 0.03	97 ± 1	0.25 ± 0.01
20	82 ± 1	0.16 ± 0.01	71 ± 1	0.22 ± 0.01	106 ± 2	0.33 ± 0.01
30	87 ± 1	0.18 ± 0.02	71 ± 1	0.24 ± 0.01	112 ± 2	0.37 ± 0.02
40	87 ± 1	0.17 ± 0.01	73 ± 1	0.28 ± 0.03	108 ± 2	0.34 ± 0.01

4. Conclusions

In this study 18β-GA-loaded ethosomes, glycethosomes, and glycerosomes were successfully produced using a customized 3D-printed microfluidic chip, enabling precise and highly reproducible control over particle size and PDI. The combination of FDM-based 3D printing with microfluidic technology effectively overcame the challenges associated with a cost-effective and reproducible manufacturing strategy and allowed the topical delivery of 18β-GA. The application of a QbD approach enabled the development of predictive mathematical models and design spaces for each nanocarrier type, allowing the identification of optimal formulation parameters yielding nanoparticles with customized physicochemical properties. Long-term stability studies confirmed that all optimized formulations maintained their particle size, PDI, EE and ζ-potential over 90 days. Incorporation into an alginate hydrogel imparted desirable shear-thinning rheological behavior, facilitating topical application while preserving vesicle integrity. *Ex vivo* skin permeation studies demonstrated that formulation composition significantly influenced drug delivery profiles. Ethosomes enable measurable drug delivery to the epidermis and dermis, whereas glycethosomes exhibited enhanced structural stability but more limited skin uptake, and glycerosomes achieved favorable skin permeation without the use of ethanol, supporting repeated topical application. Hydrogel formulations

further reduced drug release and skin penetration, reflecting the additional diffusional barrier introduced by the polymeric matrix. The results indicate that drug release from the formulation represents the rate-limiting step governing skin delivery, suggesting a formulation-controlled delivery mechanism. In this context, nanocarriers act as reservoir systems at the formulation level, modulating drug availability at the skin surface and supporting controlled and localized delivery. Although the developed models demonstrated good predictive capability within the defined design space and formulation conditions, their applicability to other drugs requires further experimental validation. The strength of this study lies in the generalizable QbD-based development strategy rather than in a universally predictive model. Nevertheless, the proposed framework can be readily adapted to different drugs by redefining the design space according to their specific physicochemical properties. Finally, scale-up experiments conducted with a peristaltic pump, confirmed consistent nanoparticle production, highlighting the robustness and reproducibility of the microfluidic chip and supporting its potential as a cost-effective, scalable, continuous, and industrially viable manufacturing approach for clinical translation.

CRediT authorship contribution statement

Giulia Bucciarelli: Writing – original draft, Methodology, Investigation, Formal analysis, Data curation. **Giulia Curzi:** Writing – review & editing, Supervision, Resources, Conceptualization. **Mattia Tiboni:** Writing – review & editing, Supervision, Methodology, Data curation. **Annalisa Aluigi:** Writing – review & editing, Supervision, Methodology, Data curation. **Andrea Heinz:** Writing – review & editing, Supervision, Resources, Methodology, Conceptualization. **Luca Casettari:** Writing – review & editing, Writing – original draft, Supervision, Project administration, Funding acquisition, Conceptualization.

Funding

This work has been funded by the European Union – NextGenerationEU, Mission 4, Component 2, under the Italian Ministry of University and Research (MUR) National Innovation Ecosystem grant ECS00000041 - VITALITY – CUP H33C22000430006. AH acknowledges financial support from the LEO Foundation (grant number 15007).

Declaration of competing interest

The authors declare the following financial interests/personal relationships which may be considered as potential competing interests:

Prof. Luca Casettari is cofounder and CEO of Prosopika srl.

Appendix A. Supplementary data

Supplementary data to this article can be found online at https://doi.org/10.1016/j.ijpx.2026.100563.

Data availability

Data will be made available on request.

References

Abdallah, M.H., Shahien, M.M., El-Horany, H.E.S., Ahmed, E.H., 2025. Modified Phospholipid Vesicular Gel for Transdermal Drug Delivery: The Influence of Glycerin and/or Ethanol on Their Lipid Bilayer Fluidity and Penetration Characteristics. Multidisciplinary Digital Publishing Institute (MDPI). https://doi.org/10.3390/gels11050358.

Abka-khajouei, R., Tounsi, L., Shahabi, N., Patel, A.K., Abdelkafi, S., Michaud, P., 2022. Structures, Properties and Applications of Alginates. MDPI. https://doi.org/10.3390/md20060364.

Abou-Saleh, R.H., et al., 2019. Molecular effects of glycerol on lipid monolayers at the gas-liquid interface: impact on microbubble physical and mechanical properties. Langmuir 35 (31), 10097–10105. https://doi.org/10.1021/acs.langmuir.8b04130.

Agha, A., et al., 2023. A Review on Microfluidic-assisted Nanoparticle Synthesis, and Their Applications Using Multiscale Simulation Methods. https://doi.org/10.1186/s11671-023-03792-x.

Albakr, L., et al., 2024. Progress in Lipid and Inorganic Nanocarriers for Enhanced Skin Drug Delivery. John Wiley and Sons Inc. https://doi.org/10.1002/anbr.202400003.

Andersen, F.A., 2007. Final Report on the Safety Assessment of Glycyrrhetinic Acid, Potassium Glycyrrhetinate, Disodium Succinoyl Glycyrrhetinate, Glyceryl Glycyrrhetinate, Glycyrrhetinyl Stearate, Stearyl Glycyrrhetinate, Glycyrrhizic Acid, Ammonium Glycyrrhizate, Dipotassium Glycyrrhizate, Disodium Glycyrrhizate, Trisodium Glycyrrhizate, Methyl Glycyrrhizate, and Potassium Glycyrrhizinate. https://doi.org/10.1080/10915810701351228.

Bag, B.G., Majumdar, R., 2012. Self-assembly of a renewable nano-sized triterpenoid 18β-glycyrrhetinic acid. RSC Adv. 2 (23), 8623–8626. https://doi.org/10.1039/C2RA21051G.

Bos, J.D., Meinardi, M.M.H.M., 2000. The 500 Dalton Rule for the Skin Penetration of Chemical Compounds and Drugs. https://doi.org/10.1034/j.1600-0625.2000.009003165.x.

Cai, D., et al., 2022. Injectable carrier-free hydrogel dressing with anti-multidrug-resistant staphylococcus aureus and anti-inflammatory capabilities for accelerated wound healing. ACS Appl. Mater. Interfaces 14 (38), 43035–43049. https://doi.org/10.1021/acsami.2c15463.

Chanda, J., Chakraborty, S., Bandyopadhyay, S., 2006. Sensitivity of hydrogen bond lifetime dynamics to the presence of ethanol at the interface of a phospholipid bilayer. J. Phys. Chem. B 110 (8), 3791–3797. https://doi.org/10.1021/jp054275i.

Coderch, L., Collini, I., Carrer, V., Barba, C., Alonso, C., 2021. Assessment of finite and infinite dose in vitro experiments in transdermal drug delivery. Pharmaceutics 13 (3). https://doi.org/10.3390/pharmaceutics13030364.

Danaei, M., et al., 2018. Impact of Particle Size and Polydispersity Index on the Clinical Applications of Lipidic Nanocarrier Systems. MDPI AG. https://doi.org/10.3390/pharmaceutics10020057.

Duarte, L.C., Figueredo, F., Chagas, C.L.S., Cortón, E., Coltro, W.K.T., 2024. A Review of the Recent Achievements and Future Trends on 3D Printed Microfluidic Devices for Bioanalytical Applications, Elsevier B.V. https://doi.org/10.1016/j.aca.2024.342429.

E. Medicines Agency, 2014. Committee for Medicinal Products for Human Use (CHMP) Guideline on Quality of Transdermal Patches. https://www.ema.europa.eu/en/quality-transdermal-patches-scientific-guideline.

Fda, Cder, 2026. In Vitro Permeation Test Studies for Topical Drug Products Submitted in ANDAs. https://www.fda.gov/regulatory-information/search-fda-guidance-documents/in-vitro-permeation-test-studies-topical-drug-products-submitted-andas.

Fluhr, J.W., Feingold, K.R., Elias, P.M., 2006. Transepidermal water loss reflects permeability barrier status: validation in human and rodent in vivo and ex vivo models. Exp. Dermatol. 15 (7), 483–492. https://doi.org/10.1111/j.1600-0625.2006.00437.x.

Grijalvo, S., Mayr, J., Eritja, R., Díaz, D.D., 2016. Biodegradable Liposome-encapsulated Hydrogels for Biomedical Applications: A Marriage of Convenience. Royal Society of Chemistry. https://doi.org/10.1039/C5BM00481K.

Gupta, P., Mazumder, R., Padhi, S., 2020a. Glycerosomes: Advanced Liposomal Drug Delivery System. Indian Pharmaceutical Association. https://doi.org/10.36468/PHARMACEUTICAL-SCIENCES.661.

Gupta, R., Badhe, Y., Rai, B., Mitragotri, S., 2020b. Molecular mechanism of the skin permeation enhancing effect of ethanol: a molecular dynamics study. RSC Adv. 10 (21), 12234–12248. http://xlink.rsc.org/?DOI=d0ra01692f.

Kong, S.Z., et al., 2015. The protective effect of 18β-Glycyrrhetinic acid against UV irradiation induced photoaging in mice. Exp. Gerontol. 61, 147–155. https://doi.org/10.1016/j.exger.2014.12.008.

Kowalska, A., Kalinowska-Lis, U., 2019. 18β-Glycyrrhetinic Acid: Its Core Biological Properties and Dermatological Applications, Blackwell Publishing Ltd. https://doi.org/10.1111/ics.12548.

Levin, J., Maibach, H., 2005. The Correlation Between Transepidermal Water Loss and Percutaneous Absorption: An Overview. https://doi.org/10.1016/j.jconrel.2004.11.035.

Li, X., Sun, R., Liu, R., 2019. Natural Products in Licorice for the Therapy of Liver Diseases: Progress and Future Opportunities, Academic Press. https://doi.org/10.1016/j.phrs.2019.04.025.

Lin, X., et al., 2024. Self-assembly variation of glycyrrhetinic acid epimers: assembly mechanism and antibacterial efficacy between 18 α-GA and 18 β-GA. Colloids Surf. B Biointerfaces 242. https://doi.org/10.1016/j.colsurfb.2024.114120.

Manca, M.L., et al., 2013. Glycerosomes: a new tool for effective dermal and transdermal drug delivery. Int. J. Pharm. 455 (1–2), 66–74. https://doi.org/10.1016/j.ijpharm.2013.07.060.

Manca, M.L., et al., 2019. Optimization of innovative three-dimensionally-structured hybrid vesicles to improve the cutaneous delivery of clotrimazole for the treatment of topical candidiasis. Pharmaceutics 11 (6). https://doi.org/10.3390/pharmaceutics11060263.

Montgomery, D.C., 2017. Design and Analysis of Experiments, 9th edition. Wiley.

Neupane, R., Boddu, S.H.S., Renukuntla, J., Babu, R.J., Tiwari, A.K., 2020. Alternatives to Biological Skin in Permeation Studies: Current Trends and Possibilities. MDPI AG. https://doi.org/10.3390/pharmaceutics12020152.

OECD, 2004. S. 4 OECD Guidelines for the Testing of Chemicals, Test No. 428: Skin Absorption: In Vitro Method. Paris, 2004. https://doi.org/10.1787/9789264071087-en.

Oh, L., Yi, S., Zhang, D., Shin, S.H., Bashaw, E., 2020. In Vitro Skin Permeation Methodology for Over-The-Counter Topical Dermatologic Products. Springer Science and Business Media Deutschland GmbH. https://doi.org/10.1007/s43441-019-00104-3.

Pastorino, G., Cornara, L., Soares, S., Rodrigues, F., Oliveira, M.B.P.P., 2018. Liquorice (Glycyrrhiza glabra): A Phytochemical and Pharmacological Review, John Wiley and Sons Ltd. https://doi.org/10.1002/ptr.6178.

Peralta, M.F., et al., 2018. Liposomes can both enhance or reduce drugs penetration through the skin. Sci. Rep. 8 (1). https://doi.org/10.1038/s41598-018-31693-y.

Pleguezuelos-Villa, M., et al., 2020. Mangiferin glycethosomes as a new potential adjuvant for the treatment of psoriasis. Int. J. Pharm. 573. https://doi.org/10.1016/j.ijpharm.2019.118844.

Prow, T.W., et al., 2011. Nanoparticles and Microparticles for Skin Drug Delivery. https://doi.org/10.1016/j.addr.2011.01.012.

Quan, W., et al., 2021. Use of 18β-glycyrrhetinic acid nanocrystals to enhance anti-inflammatory activity by improving topical delivery. Colloids Surf. B Biointerfaces 205. https://doi.org/10.1016/j.colsurfb.2021.111791.

Rahali, K., Tabriz, A.G., Douroumis, D., 2024. The effect of 3D printed microfluidic array designs on the preparation of liposome nanoparticles. J. Drug Deliv. Sci. Technol. 94. https://doi.org/10.1016/j.jddst.2024.105411.

Raina, N., Rani, R., Thakur, V.K., Gupta, M., 2023. New Insights in Topical Drug Delivery for Skin Disorders: From a Nanotechnological Perspective. American Chemical Society. https://doi.org/10.1021/acsomega.2c08016

Saha, A., Adamcik, J., Bolisetty, S., Handschin, S., Mezzenga, R., 2015. Fibrillar networks of glycyrrhizic acid for hybrid nanomaterials with catalytic features. Angew. Chem. 127 (18), 5498–5502. https://doi.org/10.1002/ange.201411875.

Sharma, D., Rani, A., Singh, V.D., Shah, P., Sharma, S., Kumar, S., 2023. Glycerosomes: Novel Nano-vesicles for Efficient Delivery of Therapeutics. Bentham Science Publishers. https://doi.org/10.2174/0126673878245185230919101148.

Shinu, P., et al., 2023. Pharmacological Features of 18β-Glycyrrhetinic Acid: A Pentacyclic Triterpenoid of Therapeutic Potential, MDPI. https://doi.org/10.3390/plants12051086.

Su, R., Wang, F., McAlpine, M.C., 2023. 3D Printed Microfluidics: Advances in Strategies, Integration, and Applications, Royal Society of Chemistry. https://doi.org/10.1039/d2lc01177h.

Summerfield, A., Meurens, F., Ricklin, M.E., 2015. The Immunology of the Porcine Skin and Its Value as a Model for Human Skin, Elsevier Ltd. https://doi.org/10.1016/j.molimm.2014.10.023.

Sun, Y., Dai, C., Yin, M., Lu, J., Hu, H., Chen, D., 2018. Hepatocellular carcinoma-targeted effect of configurations and groups of glycyrrhetinic acid by evaluation of its derivative-modified liposomes. Int. J. Nanomedicine 13, 1621–1632. https://doi.org/10.2147/IJN.S153944.

Tiboni, M., et al., 2020. 3D-printed microfluidic chip for the preparation of glycyrrhetinic acid-loaded ethanolic liposomes. Int. J. Pharm. 584. https://doi.org/10.1016/j.ijpharm.2020.119436.

Tiboni, M., et al., 2021. Microfluidics for nanomedicines manufacturing: an affordable and low-cost 3D printing approach. Int. J. Pharm. 599. https://doi.org/10.1016/j.ijpharm.2021.120464.

Verma, P., Pathak, K., 2010. Therapeutic and Cosmeceutical Potential of Ethosomes: An Overview, Wolters Kluwer Medknow Publications. https://doi.org/10.4103/0110-5558.72415.

Verratti, E., et al., 2011. 18β-Glycyrrhetinic Acid and Glabridin prevent oxidative DNA fragmentation in UVB-irradiated human keratinocyte cultures. Anticancer Res. 6, 2209–2215.

Wang, W., Luo, M., Fu, Y., Wang, S., Efferth, T., Zu, Y., 2013. Glycyrrhizic acid nanoparticles inhibit LPS-induced inflammatory mediators in 264.7 mouse macrophages compared with unprocessed glycyrrhizic acid. Int. J. Nanomedicine 8, 1377–1383. https://doi.org/10.2147/ijn.s37788.

Wang, Z., Chen, R., Chen, J., Su, L., 2024. 18β-glycyrrhetinic acid alleviates radiation-induced skin injury by activating the Nrf2/HO-1 signaling pathway. Biol. Chem. 405 (6), 407–415. https://doi.org/10.1515/hsz-2023-0200.

Xu, J., Harasek, M., Gföhler, M., 2025. From Soft Lithography to 3D Printing: Current Status and Future of Microfluidic Device Fabrication, Multidisciplinary Digital Publishing Institute (MDPI). https://doi.org/10.3390/polym17040455.

Yamaguchi, H., et al., 2010. Novel effects of glycyrrhetinic acid on the central nervous system tumorigenic progenitor cells: induction of actin disruption and tumor cell-selective toxicity. Eur. J. Med. Chem. 45 (7), 2943–2948. https://doi.org/10.1016/j.ejmech.2010.03.021.

Zahid, S.R., Upmanyu, N., Dangi, S., Ray, S.K., Jain, P., Parkhe, G., 2018. Ethosome: a novel vesicular carrier for transdermal drug delivery. J. Drug Deliv. Ther. 8 (6), 318–326. https://doi.org/10.22270/jddt.v8i6.2028.

Zhang, Y.Q., Liang, R., Liu, C., Yang, C., 2022. Improved stability and skin penetration through glycethosomes loaded with glycyrrhetinic acid. Int. J. Cosmet. Sci. 44 (2), 249–261. https://doi.org/10.1111/ics.12771.

Zhang, H., Yang, J., Sun, R., Han, S., Yang, Z., Teng, L., 2023. Microfluidics for Nano-drug Delivery Systems: From Fundamentals to Industrialization. Chinese Academy of Medical Sciences. https://doi.org/10.1016/j.apsb.2023.01.018.